Research Square

Preprints are preliminary reports that have not undergone peer review.
They should not be considered conclusive, used to inform clinical practice,
or referenced by the media as validated information.

The Effect of Parameters of Ziegler-Natta Catalyst on the Polymerization Kinetics and Polyethylene Properties

Ehsan Nikzinat

e.nikzinat@jpcomplex.com

Jam Petrochemical Company

Abdolhannan Sepahi

Jam Petrochemical Company

Shahin Hosseini

Jam Petrochemical Company

Mohammad Hossein Jandaghian

Amirkabir University of Technology

Saeed Houshmandmoaye

Jam Petrochemical Company

Hossein Bazgir

Jam Petrochemical Company

Maryam Masoori

Jam Petrochemical Company

Research Article

Keywords: Polyethylene, Ziegler-Natta Catalyst, Pre-polymerization, polymerization Kinetics, and Physical-Mechanical Properties

Posted Date: June 30th, 2026

DOI: https://doi.org/10.21203/rs.3.rs-10056069/v1

License: This work is licensed under a Creative Commons Attribution 4.0 International License.
Read Full License

Additional Declarations: No competing interests reported.

Abstract

In this study, three industrial $TiCl_4/MgCl_2$-based Ziegler–Natta catalysts were investigated to clarify how their physicochemical characteristics influence polymerization behavior and the resulting polyethylene properties. Catalyst composition, porosity, and particle morphology were evaluated using standard characterization techniques. Ethylene polymerization was performed under two experimental modes: first, with equal catalyst loading to compare intrinsic catalytic performance; and second, with adjusted catalyst amounts to produce polyethylene samples of similar yield for a more reliable comparison of polymer properties. Polymer characteristics, including melt flow index (MFI), flow rate ratio (FRR), differential scanning calorimetry (DSC), density, and particle size distribution, were assessed to investigate hydrogen response, comonomer response, and polymer morphology. Additionally, propylene pre-polymerization was carried out to study its influence on catalyst behavior and to simulate industrial pre-polymerization practices. Overall, this work establishes clear correlations between catalyst structure, polymerization kinetics, and polyethylene properties and highlights the potential of pre-polymerization as a strategy to tune the performance of industrial Ziegler–Natta catalysts.

Introduction

Over the past few decades, polyethylene has been the most widely used polymer worldwide, with various applications including pipes, films, injection-molded parts, and other polymer-forming processes [1, 2]. Polyethylene can be produced either via radical polymerization or through catalytic routes such as Ziegler-Natta coordination catalysts. These catalysts usually have a magnesium support and active sites of titanium ($TiCl_4/MgCl_2$) [3–5]. In the manufacture of catalysts, various methods are used to form the support, including physical methods such as jet mill, ball mill, and gelation, and chemicals such as alkylation and dealcoholization [6, 7]. After that, active sites are formed by the addition of titanium compounds such as titanium tetrachloride or titanium tetrabutoxide [5, 8]. The presence of electron donors or promoters, which include metal compounds such as the chlorine compounds of zinc, iron, silicon, also has a great influence on the activity of the catalyst and the properties of the final polymer [9].

The morphology of the catalysts can be either spherical or amorphous, and their shape influences the morphology of the resulting polymer powder [10]. Also, the presence of cracks on the catalysts and the catalyst particle strength determines the possibility of fragmentation. The lower strength of the catalyst and the greater fragmentation prohibit the efficiency and limit the application of the catalyst. Because excessive fragmentation of the catalyst is not allowed on an industrial scale due to the problems such as chunk formation, fouling and polymer lumps either in the reactor or transfer lines [11–13]. On the other hand, overly strength of the catalysts prevents the growth of the polymer particle and decrease the activity of the catalyst [14]. Moreover, the pore sizes and surface characteristics of the catalyst also govern the activity of the catalyst and the comonomer response. The smaller pore diameters restrict comonomer diffusion, which explains the lower participation of the 1-hexene compared to 1-butene in polyethylene chains due to 1-hexene molecule larger size [15, 16].

The Ti content of the catalyst has an optimal value, below which causes a decrease in the number of active sites and activity, while excessive Ti content results in the formation of Ti accumulations that interfere with other sites and reduce the activity of the catalyst [17]. The presence of other elements further influences the activity of the catalyst, hydrogen response, comonomer response, molecular weight and molecular weight distribution, the polymer particle size and its distribution, as well as the amount of wax [18–20]. The presence of different elements causes such changes due to their ionic charge and crystal structure. Even the distribution of elements on the surface and inside the catalyst can be different, which causes differences in the catalyst activity on the onset and progression of the reaction; because initially, the surface of the catalyst is attainable, and as the polymerization proceeds, with the opening of the catalyst, internal pores become accessible. In other words, the rate of the reaction at beginning stage indicates the surface characteristics of the catalyst, while its proceeding depends on its internal sites conditions [21]. In addition, at the beginning of the reaction, the catalyst sites are more accessible for the comonomer. By the progress of the polymerization and the formation of polymer on the surface and inside the catalyst, the penetration of monomer and comonomer decreases. It is crystal clear that larger size of comonomer molecule in comparison with the ethylene, causes more restrictions on the comonomer penetration, and consequently, less comonomer response, as the polymerization proceeds [11, 22, 23].

Before ethylene polymerization, pre-polymerization with propylene is sometimes carried out, and internal and external electron donors are used to control and increase the tacticity of the formed polypropylene [24]. Atactic polypropylene is amorphous and soluble in hydrocarbon solvents, so in ethylene polymerization, the atactic polypropylene content is more crucial than other tacticity structures. A lower fraction of atactic structure results in the less part of the polymer soluble in xylene, which reduces operational problems in polymerization reactors, conveying lines, and downstream polymer processing [25–27].

In this study, three $TiCl_4/MgCl_2$ Ziegler-Natta catalysts were investigated to establish the relationship among catalyst characteristics, polymerization behavior, and the resulting polymer properties, to have a better prediction of a Ziegler-Natta catalyst reaction behavior under industrially operational conditions. The investigation includes elemental analysis of the catalyst surface and within the catalyst particles, porosity, and the catalyst particles size and morphology. The polymerization performance of the catalysts with ethylene and propylene was evaluated, and the properties of the produced polymers were compared in terms of catalyst activity, hydrogen response, comonomer response, wax formation, and other performance indicators of the catalysts.

Experimental

Materials

N-hexane, which was used as the polymerization medium, ultra-pure ethylene gas (purity > 99.9%), and three industrial types of Ziegler-Natta catalyst (P1, F0, and F0A) were provided by JAM Petrochemical

Company (JPC). A 1 molar triethylaluminium (TEA) solution in hexane and the ultra-pure hydrogen gas (purity > 99.999%) were purchased from Sigma Aldrich and Farafan Gas Co., respectively.

Polymerization

Ethylene/1-butene copolymerization was carried out in a 1 L steel reactor equipped with a mechanical agitator and a high-pressure catalyst/cocatalyst injection system. The polymerization temperature was automatically controlled via an oil-circulation jacket between inner and outer reactor walls. Ethylene consumption during the polymerization reaction was compensated by using an ethylene gas stream into the reactor, through a mass flow controller, to maintain constant pressure.

In a typical monomodal copolymerization run, 650 mL n-hexane was charged into the reactor under a nitrogen atmosphere at 40 ℃. After degassing the reactor and adding 1-butene into the reactor, the mixture was heated up to the reaction temperature while agitated at 400 rpm. A specified pressure of hydrogen and ethylene gases was introduced into the reactor, respectively. Subsequently, the TEA solution was injected into the reactor by using 20 mL of high-pressure n-hexane through the injection port. The polymerization started upon the catalyst injection with a procedure similar to the TEA addition. The reaction was carried out, and the curve of ethylene uptake was recorded, simultaneously. As the reaction complete, the gases were vented, and the reactor was cooled down to 50 ℃ under mild agitation. Finally, polyethylene powder was collected and dried at 80 ℃ and 400 mmHg overnight.

Characterization

Metal contents of the solid catalysts were determined using the inductively coupled plasma (ICP) technique with an Agilent (model: 5800 ICP-OES) instrument. Samples were dissolved in an acidic solvent prior to analysis.

Field emission scanning electron microscopy (FE-SEM) and energy-dispersive X-ray spectroscopy (EDS or EDAX) analyses of the samples were applied to investigate the morphology and elemental composition of the catalysts' surfaces, which performed using a device made by TESCAN (model: MIRA3-XMU). To improve surface conductivity of the catalyst samples, the samples were coated by a thin layer of gold before the FE-SEM imaging.

Surface area and pore structure of the catalyst samples were measured using the Brunauer–Emmett–Teller (BET) method by a BELSORP instrument (model: Mini II).

Polyethylene powders were characterized by their melt flow index (MFI) and flow rate ratio ($FRR=MFI_{21.6}/MFI_{2.16}$). MFI analysis was performed using 2.16 kg and 21.6 kg loads at 190 ℃ according to ASTM-D1238 by a multi-weight melt flow tester (CEAST MMF Multiweight 7028). In advanced of the MFI measuring, the samples were mixed with 1500 ppm of Tetrakis [methylene-3-(3,5-di-tert-butyl-4-

hydroxyphenylpropionate)] methane (Irganox1010) and 1500 ppm of Tris (2,4-di-tert-butyl phenyl) phosphite (Irgafos 168), as antioxidants.

Differential scanning calorimetry (DSC) tests were carried out using a METTLER TOLEDO (DSC822e) instrument at a rate of 10 ℃/min. The second heating cycle from 25 to 190 ℃ was used for analysis to determine melting temperature (T_m) and crystallinity (X_c).

The density of the samples was measured by the density gradient technique according to ASTM D1505, using a calibrated column available in the JAM Petrochemical Central Lab.

The particle size distribution (PSD) of powders was determined by a Malvern (Mastersizer 2000) particle size analyzer, which was served by nitrogen gas as a fluidizing medium of polyethylene powder. For catalyst powder, n-hexane was employed as a diluent, following ISO 13320. Three main parameters d_{10}, d_{50}, and d_{90} indicate that 10%, 50%, and 90% of powder sample volume are below the corresponding diameters, respectively. The Span value, defined as $(d_{90}-d_{10})/d_{50}$, was used to describe the width of the PSD.

Xylene soluble content of polypropylene was determined according to ASTM D5492 to quantify the fraction of atactic polypropylene, which is amorphous and non-crystallizable.

Results and Discussions

Catalyst analysis

To establish the relationships among catalyst characteristics, polymerization behavior, and polyethylene properties, the catalysts were analyzed using ICP-OES, BET, DLS, FE-SEM, and EDS. Among these techniques, ICP-OES provides the most reliable quantification of elemental compositions. In Table 1, identified metals and their proportions are presented. All catalysts contained magnesium (Mg) in their formulation, which confirmed similar supports were available in their structures. Although catalysts P1 and F0 contained similar titanium (Ti) levels, they differed in their iron (Fe) contents. The F0A catalyst showed the highest Ti content among all samples. Higher Ti contents generally enhance catalyst activity; however, excessive Ti can adversely affect polymerization performance by generating inactive Ti-rich domains [28]. Another notable observation from Table 1 is the presence of silicon (Si) in catalyst F0, which is absent in P1 and F0A. Silicon- and iron-containing compounds are often introduced during catalyst preparation in the form of chlorides (e.g., $FeCl_3$, $SiCl_4$) as promoters, whose role is participating in the design of the polymer's microstructure. For example, it has been proven that $FeCl_3$, due to its relatively similar atomic radius to magnesium but a stronger electron-withdrawing ability, can partially substitute for magnesium in the support structure, which leads to the induction of a more positive charge to the active center and consequently, enhances the incorporation of 1-butene relative to ethylene. Because the double bond in 1-Butene is more electron-rich in comparison to ethylene. Therefore, by adding $FeCl_3$, the presence of 1-Butene in the polymer chain and the comonomer response

increase. A similar mechanism has been proposed for $SiCl_4$, particularly in controlling comonomer incorporation and limiting wax formation during polymerization [28–31].

Table 1
Elements of the catalysts that have been analyzed by ICP analysis

Elements	P1	F0	F0A
Ti (wt.%)	2.37	2.36	3.27
Mg (wt.%)	15.4	15.5	15.7
Ti/Mg	0.154	0.152	0.208
Fe (wt.%)	0.015	0.51	0.08
Si (wt.%)	< 0.001	0.14	< 0.001

The BET results are summarized in Table 2. The F0 catalyst exhibits significantly lower surface area and total pore volume compared to the other catalysts, indicating a more rigid structure with reduced porosity. Such differences can influence polymer morphology; therefore, to further examine their effects on polymer structure and final properties, polyethylene samples prepared on a laboratory scale were evaluated.

Table 2
Porosity characteristics of the catalysts determined by BET analysis

Catalyst	Surf.*	TPV**	APD***
P1	299.5	0.291	3.88
F0	165.7	0.154	3.71
F0A	315.0	0.293	3.72
*: Surface (m2/g); **: Total Pore Volume (Cm3/g); ***: Average Pore Diameter (nm)			

The particle size and size distribution of the catalysts strongly affect the morphology of the resulting polymer powder. Moreover, they influence catalyst activity by altering the accessible specific surface area for polymerization. As shown in Table 3, catalyst F0A possesses a considerably smaller particle size together with a broader size distribution relative to F0 and P1. Consequently, during polymerization, a greater number of F0A active centers are expected to be exposed to monomers and comonomers, leading to higher polymerization activity. In addition, smaller polymer particles are anticipated when using the F0A catalyst compared with the other samples.

Table 3
Particle size distribution of the catalysts determined by DLS analysis

Catalyst	D_{ave} (µm)	D_{50} (µm)	Span	Surface (m^2/cm^3)
P1	44.70	40.60	1.68	0.28
F0	34.12	22.37	3.76	0.78
F0A	18.94	7.25	7.06	1.14

Table 4 presents the normalized mole fractions of catalyst elements relative to magnesium obtained from EDS analysis. Higher concentrations of titanium and chlorine on the catalyst surface correspond to an increased number of active sites available at the onset of polymerization. The FE-SEM images of the catalysts (Fig. 1-Figure 3) further support these findings and are consistent with the elemental analysis.

Table 4
Mole ratio of the elements of the catalysts that have been analyzed by EDS analysis

Elements Ratio	P1	F0	F0A
[Ti]/[Mg]	0.076	0.041	0.112
[O]/[Mg]	3.054	3.889	3.312
[Cl]/[Mg]	1.953	1.508	2.146
[Al]/[Mg]	0.036	< 0.001	0.036
[Fe]/[Mg]	0.004	< 0.001	0.004
[Si]/[Mg]	0.035	< 0.001	0.026

Polymerization and polymer properties

To compare the performance of the F0 and F0A catalysts, ethylene copolymerization was carried out in the presence of a fixed amount of 1-butene (Table 5).

Table 5
Polymerization parameters for F0 and F0A catalysts

Parameters	Values of Polymerization (F0)	Values of Polymerization (F0A)
Catalyst (mg)	14	8 and 14
TEA (mg)	102.6	57 and 102.6
Ethylene (barg)	5	5
Hydrogen (barg)	3	3
1-Butene (g)	5	5

At the onset of polymerization, F0A exhibited abnormal kinetic behavior, as shown in Fig. 4a. Although the catalyst and cocatalyst amounts for polymerization of F0A catalyst were reduced by nearly 43% to achieve comparable amount of polymer, this adjustment did not eliminate the unusual kinetic peak observed between 2000 and 4000 seconds.

The higher activity of F0A and the smaller particle size of the produced polymer with this catalyst (Fig. 4b) reflect its greater fragmentation and increased exposure of active sites during polymerization. Although F0A clearly shows higher activity, its reaction intensity is unstable at the onset, making it more challenging to control the polymerization behavior. These observations are consistent with the catalyst characteristics obtained from DLS (smaller catalyst particle size), as well as the elemental analysis results from EDS and ICP.

In contrast, the polymerization of F0 proceeds more uniformly, with a pronounced reaction rate at the beginning followed by a gradual decrease as polymerization progresses. Because the average pore diameters of the catalysts are nearly identical (Table 2), changes in polymer density, lamellar thickness, and crystallinity are not expected to be significant.

Table 6
The parameters of produced polymers by different catalysts

Catalyst	Activity (kg PE/g Cat.)	$MFI_{2.16}$ (g/10min)	FRR ($MFI_{21.6}/MFI_{2.16}$)	Density (g/cm^3)	T_m (℃)	X_c (wt.%)	T_c (℃)
F0	10.4	2.2	25.7	0.9472	128.79	59.80	116.43
F0A	21.4	4.2	28.1	0.9489	128.91	62.46	116.75
F0A (57%)	24.2	1.9	28.0	0.9461	129.09	59.57	116.61

The abnormal kinetic peak observed for the F0A catalyst originates from its exceptionally high initial reaction intensity during the first hour of polymerization. Two strategies can be employed to stabilize this behavior. First, pre-polymerization of the catalyst with propylene can coat the catalyst surface with

polypropylene, thereby restricting ethylene diffusion into the pores and moderating the reaction rate. Second, increasing the hydrogen-to-ethylene ratio (H_2/C_2) decreases the local ethylene concentration near the active sites, which helps to suppress the sharp kinetic peak.

Accordingly, the optimal aluminum-to-titanium molar ratio (Al/Ti) for the F0A catalyst was investigated (Table 7), along with the influence of elevated H_2/C_2 ratios on polymerization kinetics. As shown in Fig. 5 and Table 8, the cocatalyst-to-catalyst ratios required for P1 and F0A are comparable. However, the optimal Al/Ti ratio for F0A is lower than that of P1 due to the higher Ti content in the F0A catalyst. At higher H_2/C_2 ratios, the onset peak in the kinetic profile of F0A is considerably reduced, enabling the production of injection-molding grade high-density polyethylene. As illustrated in Fig. 5, the kinetic behavior of F0A at elevated H_2/C_2 ratios is significantly improved. Furthermore, the activity of the F0A catalyst under these conditions is approximately 43.7–54.4% higher than that of P1 across several Al/Ti ratios. Then, the activity of F0A in MFI results in about 17 g/10min must be higher than the measured quantities of Table 8. The optimum of Al/Ti ratio is 75 based on activity, MFI, and density results.

Table 7
Parameters of polymerization with higher H_2/C_2

Parameters	**Values of Polymerization (P1)**	**Values of Polymerization (F0A)**
Round (RPM)	400	400
Catalyst (mg)	14	8
TEA (mg)	102.6	57,68.4, and 102.6
Temperature (℃)	80	80
Pressure (barg)	8.5	8.5
Hexane (ml)	670	670
Ethylene (barg)	3.73	3.47
Hydrogen (barg)	4.27	4.53
1-Butene (g)	2.5	2.5
Time (h)	3.5	3.5

Table 8
Properties of the produced experimental injection-molding grade high-density polyethylene by P1 and F0A catalysts

Batch NO.	TEA (mg)	Cat. (mg)	Product (g)	Activity (tonPE/kgCat/h)	Relative Activity	$MFI_{2.16}$ (g/10min)	Density (g/cm3)
P1 (Al/Ti = 120)	102.6	14	156.261	3.189	1	17.055	0.9536
F0A (Al/Ti = 55)	57	8	130.241	4.651	1.458	22.437	0.9557
F0A (Al/Ti = 75)	68.4	8	137.867	4.924	1.544	21.256	0.9538
F0A (Al/Ti = 120)	102.6	8	128.334	4.583	1.437	21.381	0.9552

Before applying pre-polymerization to the catalysts, their propylene response was evaluated under the conditions listed in Table 9. Two values of catalyst weight were investigated for F0A. The results show that the polyethylene yield at lower catalyst weight for F0A was proportional to that obtained with P1 under comparable conditions. TEA and C-donor concentrations were also varied according to Table 9. As illustrated in Fig. 6, the propylene response of F0A was significantly lower than P1, whereas its ethylene response was higher. Furthermore, F0A exhibited greater xylene solubility than P1, indicating a larger atactic fraction and consequently increased wax formation during polymerization. Therefore, pre-polymerization of F0A presented two main challenges: reduced propylene response and increased xylene-soluble fraction.

Table 9
Pre-polymerization conditions

Parameters	Values of Pre-polymerization (P1)	Values of Pre-polymerization (F0A)
Round (RPM)	200	200
Catalyst (mg)	30	16,30
TEA (mg)	912	501.6,912
C-Donor (mg)	184.1	102.3,184.1
Temperature (℃)	65	65
Pressure (barg)	6	6
Hexane (ml)	670	670
Propylene (barg)	6	6
Time (h)	1	1
Xylene solubility (wt.%)	3.40	5.45

The final step of this work involved synthesizing polyethylene after pre-polymerization to evaluate the resulting polymer properties under the optimized conditions (Table 10). Because of the weaker propylene response and stronger ethylene response of F0A, catalyst doses of 40 mg and 28 mg were examined. According to the results summarized in Table 11, the relative activity of F0A to P1 remained approximately 1.5, and the overall kinetic trends were comparable (Fig. 7a).

However, due to its higher activity, F0A produced polymer particles with slightly larger size (Fig. 7b). Collectively, Fig. 4 and Fig. 7 indicate that pre-polymerization moderates the fragmentation behavior of F0A. The MFI, density, melting temperature, and crystallinity values of the resulting polymers were found to be similar for both catalysts.

Table 10
Pre-polymerization and polymerization conditions

Parameters	Values of Pre-polymerization	Values of Polymerization
Round (RPM)	200	400
Catalyst (mg)	40(P1), 28(F0A)	-
TEA (mg)	1208.4(P1), 843.6(F0A)	-
C-Donor (mg)	245.5(P1), 163.6(F0A)	-
Temperature (℃)	35	80
Pressure (barg)	~ 12	12
Hexane (ml)	670	-
Ethylene (barg)	-	5
Hydrogen (barg)	-	3
Propylene (g)	4.84	-
Time (min)	60	222

Table 11
Properties of produced experimental polyethylene after pre-polymerization

Batch NO.	Product (g)	Relative Activity	$MFI_{2.16}$ (g/10min)	FRR ($MFI_{21.6}/MFI_{2.16}$)	Density (g/mg)	T_m (℃)	X_c (%)
P1 (40mg)	104.66	1	1.302	27.664	0.9556	131.13	66.85
F0A (40mg)	147.32	1.408	1.154	26.872	0.9542	130.49	66.55
F0A (28mg)	121.70	1.661	1.029	26.596	0.9529	130.45	64.46

Conclusion

F0A exhibited higher titanium content and larger total surface area compared with the P1 and F0 catalyst series. The reduced level of internal donor in F0A contributed to its elevated activity during ethylene polymerization and to a stronger hydrogen response. However, these advantages were accompanied by abnormal kinetic behavior and pronounced catalyst fragmentation. Pre-polymerization of the catalyst in the presence of propylene effectively moderated these effects by partially coating the catalyst surface

and preventing extensive fragmentation during the initial stages of polymerization. As a result, the kinetic profile of F0A became more stable, and the formation of fine particles, lumps, and chunks—problems commonly encountered in industrial reactors was significantly reduced. Overall, while Ziegler–Natta catalysts containing higher titanium levels and lower internal donor content can achieve superior activity, implementing a pre-polymerization step is essential for ensuring reactor operability, controlling kinetic fluctuations, and maintaining desirable polymer particle-size distribution.

Abbreviations

Al	Aluminium
APD	Average Pore Diameter
BET	Brunauer–Emmett–Teller
Cl	Chlorine
d_{10}	10% of powder sample volume are below the corresponding diameters
d_{50}	50% of powder sample volume are below the corresponding diameters
d_{90}	90% of powder sample volume are below the corresponding diameters
DSC	Differential scanning calorimetry
EDS or EDAX	energy-dispersive X-ray spectroscopy
Fe	iron
FE-SEM	Field emission scanning electron microscopy
FRR	Flow rate ratio
ICP	inductively coupled plasma
JPC	JAM Petrochemical Company
MFI	Melt flow index
Mg	magnesium
O	Oxygen
PSD	particle size distribution
Si	silicon
SPAN	$(d_{90}-d_{10})/d_{50}$
Surf	Surface
TEA	triethylaluminium
Ti	titanium
T_m	melting temperature
TPV	Total Pore Volume
X_c	crystallinity

Declarations

Author Contribution

E.N., A.S., and S.H. wrote the main manuscript text. E.N. prepared figures and tables. All authors reviewed the manuscript.

References

1. Schwab ST, Baur M, Nelson TF, Mecking S (2024) Synthesis and deconstruction of polyethylene-type materials. Chem Rev 124(5):2327–2351
2. Burelo M, Hernández-Varela JD, Medina DI, Trevino-Quintanilla CD (2023) Recent developments in bio-based polyethylene: Degradation studies, waste management and recycling. Heliyon, *9*(11)
3. Wu Y, Li J, Ding W, Jiang T (2021) Preparation of $MgCl_2$-supported Ziegler-Natta catalysts via new surfactants emulsion for propylene polymerization. Catalysts 11(5):601
4. Udayakumar S, Ibrahim N, Chien CY, Wahab SARSA, Noor AFM, Ramakrishnan S (2020) Synthesis of Ziegler-Natta catalyst using Malaysian ilmenite derived $TiCl_4$ via recrystallization method: a statistical approach. Bull Chem Reaction Eng Catal 15(3):687–697
5. Piovano A, Signorile M, Braglia L, Torelli P, Martini A, Wada T, Groppo E (2021) Electronic properties of Ti sites in Ziegler–Natta catalysts. ACS Catal 11(15):9949–9961
6. Wu Y, Li J, Ding W, Jiang T (2021) Preparation of $MgCl_2$-supported Ziegler-Natta catalysts via new surfactants emulsion for propylene polymerization. Catalysts 11(5):601
7. Jalali Dil E, Pourmahdian S, Vatankhah M, Afshar Taromi F (2010) Effect of dealcoholation of support in $MgCl_2$-supported Ziegler–Natta catalysts on catalyst activity and polypropylene powder morphology. Polym Bull 64(5):445–457
8. Saelee T, Sitthijun P, Ngamlaor C, Kerdprasit N, Rittiruam M, Khajondetchairit P, Praserthdam S (2024) Experimental and first-principles investigation on how support morphology determines the performance of the Ziegler-Natta catalyst during ethylene polymerization. Sci Rep 14(1):17835
9. Bazgir H, Abbas-Abadi MS, Haghighi MN, Darounkola MRR, Issaabadi Z, Rashedi R (2021) Synthesis of novel Ziegler Natta catalyst in the presence of internal promoter and electron donors for ethylene and ethylene/1-hexene polymerization. J Polym Res 28(8):301
10. Werny MJ, Zarupski J, Ten Have IC, Piovano A, Hendriksen C, Friederichs NH, Weckhuysen BM (2021) Correlating the morphological evolution of individual catalyst particles to the kinetic behavior of metallocene-based ethylene polymerization catalysts. JACS Au 1(11):1996–2008
11. Fisch AG (2023) Fragmentation-oriented design of olefin polymerization catalysts: Support porosity. Catalysts 13(1):160
12. De Nicola A, Touloupidis V, Kanellopoulos V, Albunia AR, Milano G (2022) A combined experimental and molecular simulation study on stress generation phenomena during the Ziegler–Natta polyethylene catalyst fragmentation process. Nanoscale Adv 4(23):5178–5188

13. Zanoni S, Nikolopoulos N, Welle A, Vantomme A, Weckhuysen BM (2021) Early-stage particle fragmentation behavior of a commercial silica-supported metallocene catalyst. Catal Sci Technol 11(15):5335–5348
14. Jandaghian MH, Maddah Y, Sepahi A, Rashedi R, Nikzinat E, Masoori M (2022) Probing into effects of support pre-treatment on the polymerization behavior and morphology development of Mg (OEt) 2-based Ziegler–Natta catalysts. Catal Lett 152(4):1194–1204
15. Wada T, Funako T, Chammingkwan P, Thakur A, Matta A, Terano M, Taniike T (2020) Structure-performance relationship of Mg (OEt) 2-based Ziegler-Natta catalysts. J Catal 389:525–532
16. Masoori M, Rashedi R, Sepahi A, Jandaghian MH, Nikzinat E, Houshmandmoayed S (2022) Structure–Performance Relationship (SPR) of Ziegler Natta catalysts ($TiCl_4$/$MgCl_2$-based) in ethylene/1-butene and ethylene/1-hexene copolymerization. J Polym Res 29(8):317
17. Jandaghian MH, Maddah Y, Nikzinat E, Masoori M, Sepahi A, Rashedi R (2021) Investigation of the effects of heat treatment parameters during synthesis of titanium-magnesium-based Ziegler-Natta catalysts. J Macromolecular Sci Part A 58(5):287–297
18. Mehdizadeh M, Karkhaneh F, Nekoomanesh M, Sadjadi S, Emami M, Teimoury H, Posada-Pérez S (2023) Influence of the ethanol content of adduct on the Comonomer incorporation of related Ziegler–Natta catalysts in propylene (Co) polymerizations. Polymers 15(23):4476
19. Bazgir H, Abbas-Abadi MS, Haghighi MN, Darounkola MRR, Issaabadi Z, Rashedi R (2021) Synthesis of novel Ziegler Natta catalyst in the presence of internal promoter and electron donors for ethylene and ethylene/1-hexene polymerization. J Polym Res 28(8):301
20. Göpperl L, Pernusch D, Schwarz J, Paulik C (2022) Impact of Polymerization Process Parameters on Improved Comonomer Incorporation Behavior in Ziegler-Natta Catalysis. Macromol React Eng 16(2):2100042
21. Bossers KW, Valadian R, Garrevoet J, van Malderen S, Chan R, Friederichs N, Meirer F (2021) Heterogeneity in the fragmentation of ziegler catalyst particles during ethylene polymerization quantified by X-ray nanotomography. JACS Au 1(6):852–864
22. De Nicola A, Touloupidis V, Kanellopoulos V, Albunia AR, Milano G (2022) A combined experimental and molecular simulation study on stress generation phenomena during the Ziegler–Natta polyethylene catalyst fragmentation process. Nanoscale Adv 4(23):5178–5188
23. Zanoni S, Nikolopoulos N, Welle A, Vantomme A, Weckhuysen BM (2021) Early-stage particle fragmentation behavior of a commercial silica-supported metallocene catalyst. Catal Sci Technol 11(15):5335–5348
24. Osorio F, Fernández J, Bracho N, Rajmankina T (2009) Effect of external donor and prepolymerization on the performance of Ziegler-Natta catalysts in propylene polymerization. Revista Tecnica De La Facultad De Ingenieria Universidad Del Zulia 32(2):109–118
25. Gahleitner M, Tranninger C, Doshev P (2013) Heterophasic copolymers of polypropylene: Development, design principles, and future challenges. J Appl Polym Sci 130(5):3028–3037

26. Ljungberg N, Bonini C, Bortolussi F, Boisson C, Heux L, Cavaillé (2005) New nanocomposite materials reinforced with cellulose whiskers in atactic polypropylene: effect of surface and dispersion characteristics. Biomacromolecules 6(5):2732–2739
27. Gonzalez A, Eceolaza S, Etxeberria A, Iruin JJ (2007) Diffusivity of ethylene and propylene in atactic and isotactic polypropylene: Morphology effects and free-volume simulations. J Appl Polym Sci 104(6):3871–3878
28. Bazvand R, Bahri-Laleh N, Nekoomanesh M, Abedini H (2015) Highly efficient $FeCl_3$ doped Mg (OEt) 2/$TiCl_4$-based Ziegler–Natta catalysts for ethylene polymerization. Des Monomers Polym 18(7):599–610
29. Phiwkliang W (2013) Effect of lewis acid on the activity of ziegler-natta catalyst and the properties of polyethylene
30. Zhou J, Zhang X, Zhao S, Zhang Z, Ye C, Xin Z (2022) Influence of Modified Ziegler–Natta Catalyst on the Entanglement Behavior and Properties of Ultrahigh-Molecular-Weight Polyethylene (UHMWPE). Ind Eng Chem Res 61(48):17512–17523
31. Ousirisombat W (2019) Synthesis of Ziegler-Natta catalysts containing $SiCl_4$/TEOS/$TiCl_4$/$MgCl_2$ for ethylene/1-hexene copolymerization

Figures

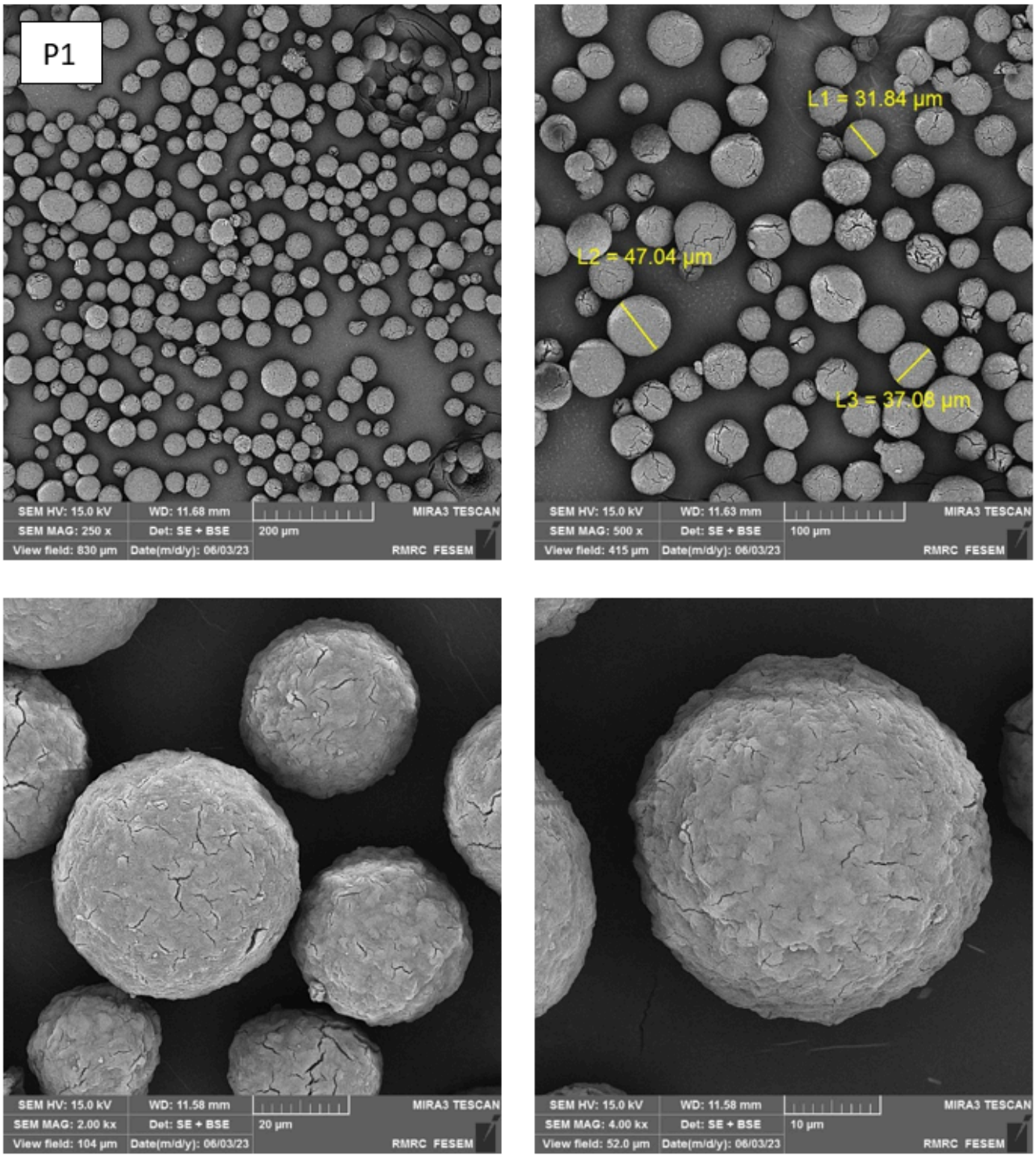


Figure 1

The FE-SEM pictures of P1 catalyst

The FE-SEM images of catalyst F0A possesses a considerably smaller particle size together with a broader size distribution relative to F0 and P1. Consequently, during polymerization, a greater number of F0A active centers are expected to be exposed to monomers and comonomers, leading to higher

polymerization activity. In addition, smaller polymer particles are anticipated when using the F0A catalyst compared with the other samples.

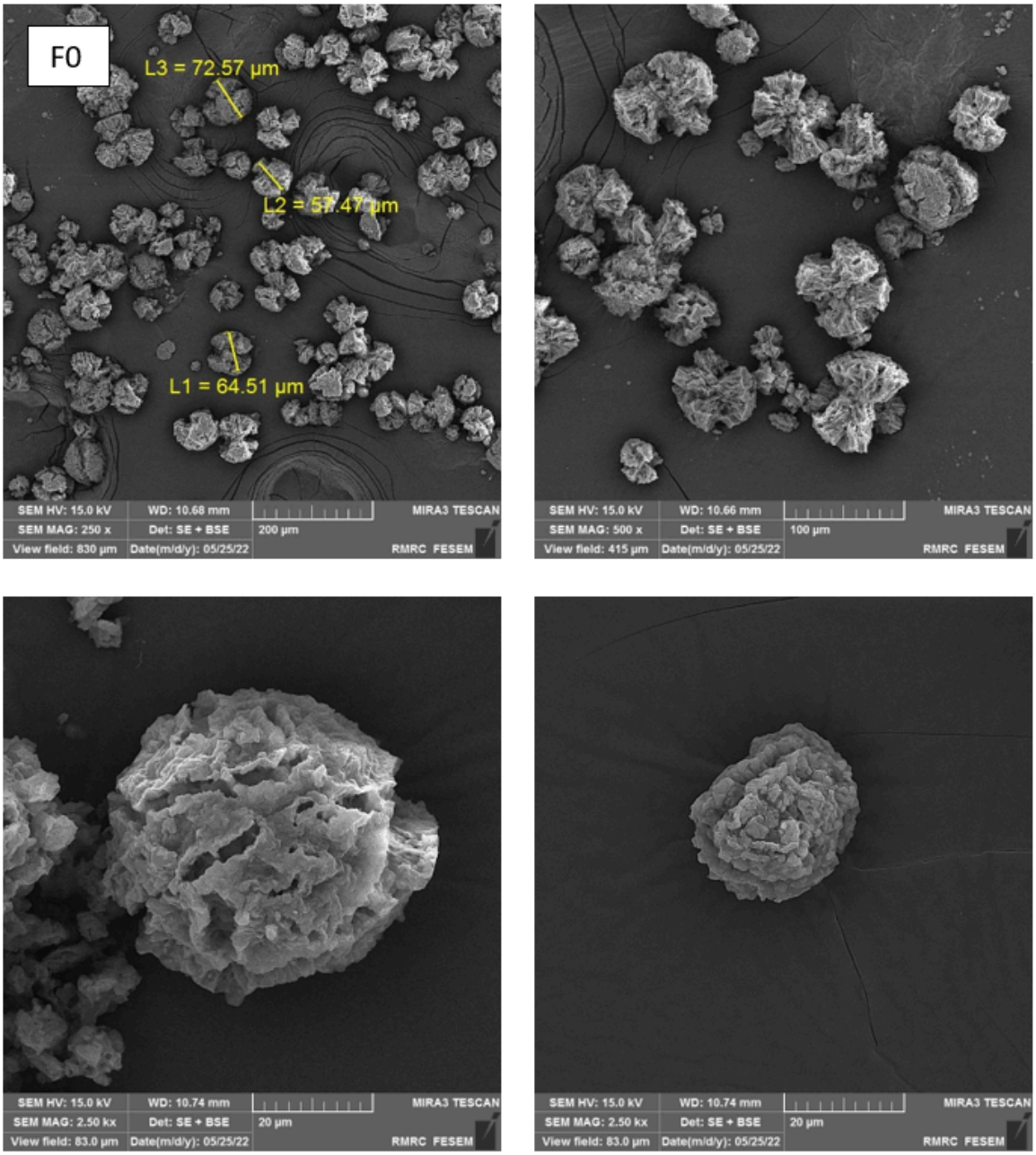


Figure 2

The FE-SEM pictures of F0 catalyst

The FE-SEM images of catalyst F0A possesses a considerably smaller particle size together with a broader size distribution relative to F0 and P1. Consequently, during polymerization, a greater number of F0A active centers are expected to be exposed to monomers and comonomers, leading to higher polymerization activity. In addition, smaller polymer particles are anticipated when using the F0A catalyst compared with the other samples.

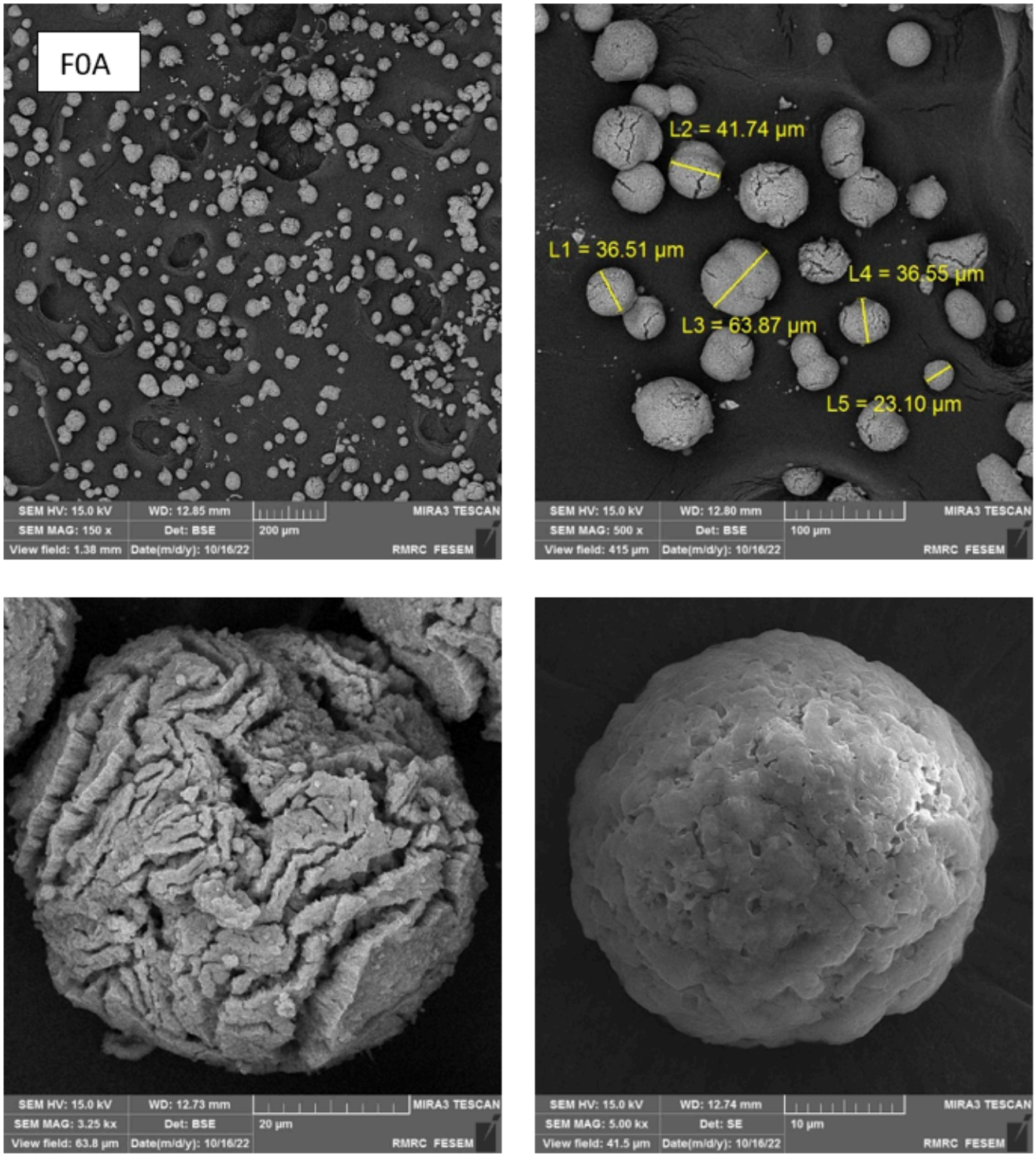


Figure 3

The FE-SEM pictures of F0A catalyst

The FE-SEM images of catalyst F0A possesses a considerably smaller particle size together with a broader size distribution relative to F0 and P1. Consequently, during polymerization, a greater number of F0A active centers are expected to be exposed to monomers and comonomers, leading to higher

polymerization activity. In addition, smaller polymer particles are anticipated when using the F0A catalyst compared with the other samples.

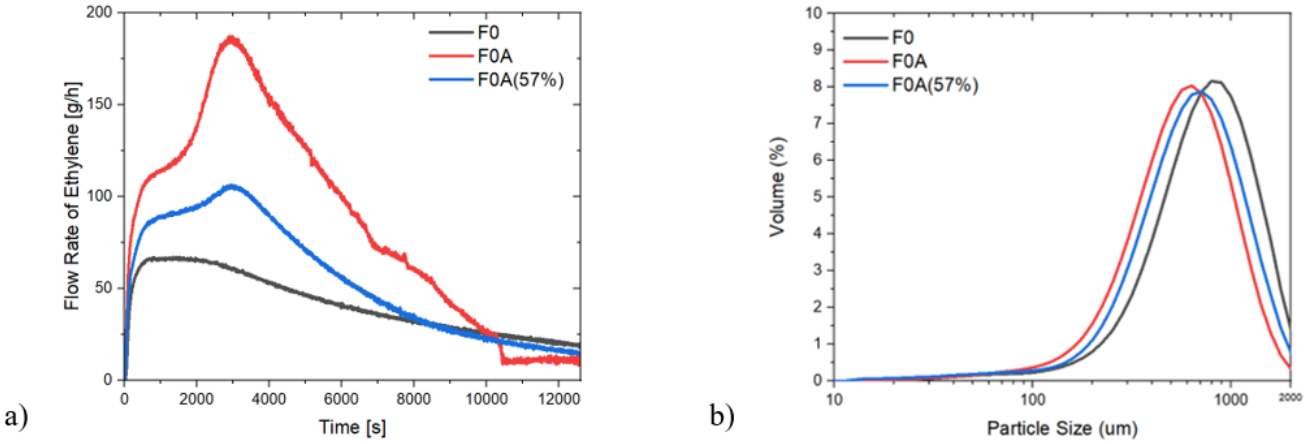


Figure 4

The comparison of a) kinetics polymerization and b) particle size distribution of F0 and F0A catalysts.

The polymerization of F0 proceeds more uniformly, with a pronounced reaction rate at the beginning followed by a gradual decrease as polymerization progresses. The abnormal kinetic peak observed for the F0A catalyst originates from its exceptionally high initial reaction intensity during the first hour of polymerization.

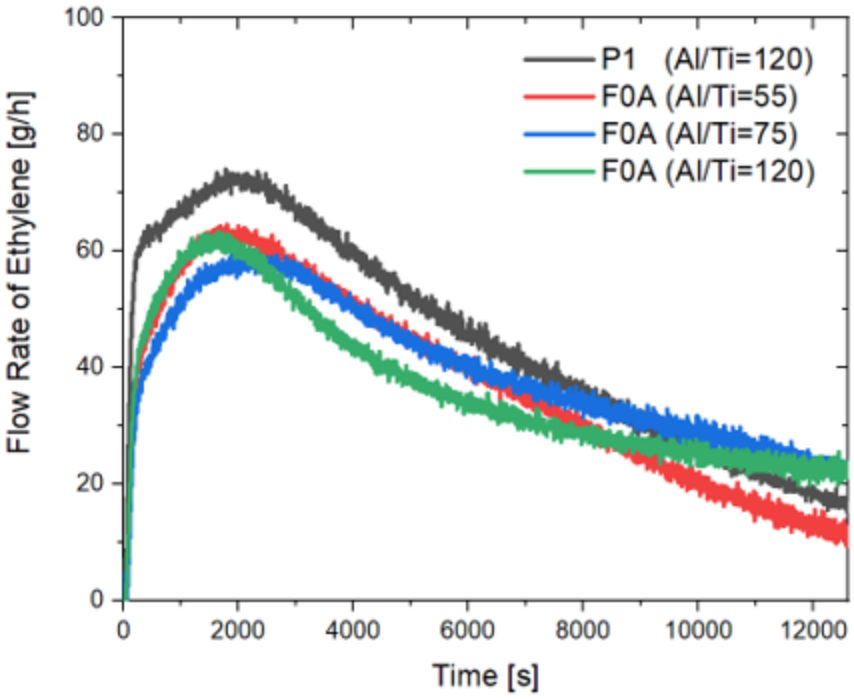


Figure 5

Kinetics of polymerization with higher H2/C2

As shown in Figure 5 and Table 8, the cocatalyst-to-catalyst ratios required for P1 and F0A are comparable. However, the optimal Al/Ti ratio for F0A is lower than that of P1 due to the higher Ti content in the F0A catalyst. At higher H_2/C_2 ratios, the onset peak in the kinetic profile of F0A is considerably reduced, enabling the production of injection-molding grade high-density polyethylene. As illustrated in Figure 5, the kinetic behavior of F0A at elevated H_2/C_2 ratios is significantly improved. Furthermore, the activity of the F0A catalyst under these conditions is approximately 43.7–54.4% higher than that of P1 across several Al/Ti ratios. Then, the activity of F0A in MFI results in about 17 g/10min must be higher than the measured quantities of Table 8. The optimum of Al/Ti ratio is 75 based on activity, MFI, and density results.

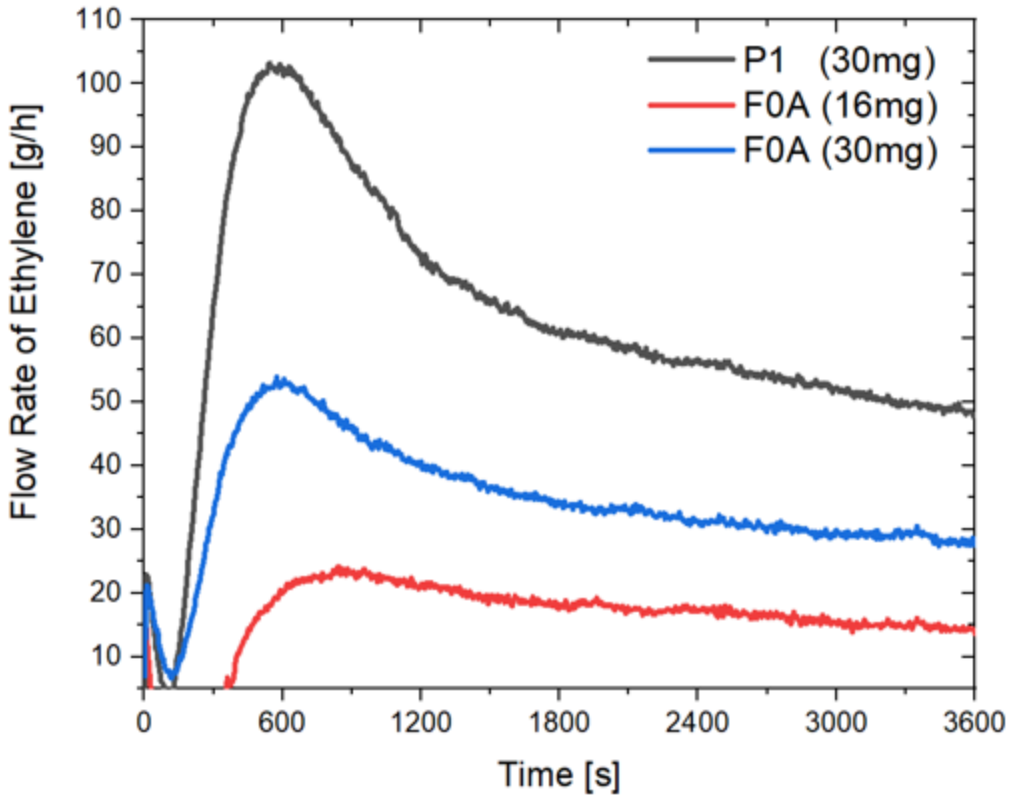


Figure 6

Pre-polymerization kinetics

As illustrated in Figure 6, the propylene response of F0A was significantly lower than P1, whereas its ethylene response was higher. Furthermore, F0A exhibited greater xylene solubility than P1, indicating a larger atactic fraction and consequently increased wax formation during polymerization.

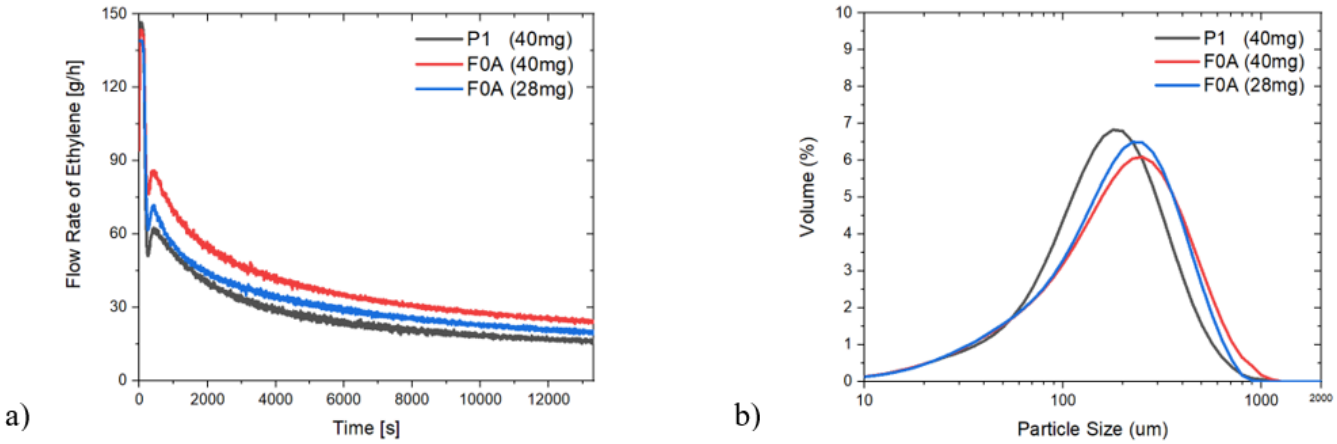


Figure 7

a) The kinetics of polymerization, b) Particle size distribution

According to the results summarized in Table 11, the relative activity of F0A to P1 remained approximately 1.5, and the overall kinetic trends were comparable (Figure 7a). However, due to its higher activity, F0A produced polymer particles with slightly larger size (Figure 7b).

Supplementary Files

This is a list of supplementary files associated with this preprint. Click to download.

- F0FESEMEDS.rar
- P1FESEMEDS.rar
- F0AFESEMEDS.rar
- GraphicalAbstract.docx